Available online at www.sciencedirect.com
ScienceDirect
Journal of Sound and Vibration 298 (2006) 855–876
JOURNAL OF SOUND AND VIBRATION
www.elsevier.com/locate/jsvi

Interaction between a railway track and uniformly moving tandem wheels

P.M. Belotserkovskiy

Department of Higher Mathematics, Moscow State University of Communications (MIIT), Obraztsov Street, 15, 127994 Moscow, Russia

Received 4 March 2004; received in revised form 15 October 2005; accepted 6 March 2006
Available online 1 September 2006

Abstract

Interaction among loaded wheels via railway track is studied. The vertical parametric oscillations of an infinite row of identical equally spaced wheels, bearing constant load and uniformly moving over a railway track, are calculated by means of Fourier series technique. If the distance between two consecutive wheels is big enough, then one can disregard their interaction via the railway track and consider every wheel as a single one. In this case, however, the Fourier series technique represents an appropriate computation time-saving approximation to a Fourier integral transformation technique that describes the oscillations of a single moving wheel. Two schemes are considered. In the first scheme, every wheel bears the same load. In the second one, consecutive wheels bear contrarily directed loads of the same magnitude. The second scheme leads to simpler calculations and so is recommended to model the wheel–track interaction.

The railway track periodicity due to sleeper spacing is taken into account. Each period is the track segment between two adjacent sleepers. A partial differential equation with constant coefficients governs the vertical oscillations of each segment. Boundary conditions bind the oscillations of two neighbour segments and provide periodicity to the track.

The shear deformation in the rail cross-section strongly influences the parametric oscillations. It also causes discontinuity of the rail centre-line slope at any point, where a concentrated transverse force is applied. Therefore, Timoshenko beam properties with respect to the topic of this paper are discussed.

Interaction between a railway track and a bogie moving at moderate speed is studied. The study points to influence of the bogie frame oscillations on variation in the wheel–rail contact force over the sleeper span. The simplified bogie model considered includes only the primary suspension. A static load applied to the bogie frame centre presents the vehicle body.

1. Introduction

Many rail systems (subways, tramways and so on) operate with rather moderate speed. However, some dynamical problems arise from their operation. Small variation in railway track vertical stiffness due to sleeper spacing causes parametric oscillations of the moving wheels and variation in the rail–wheel contact force over the sleeper span that can influence the wheel and rail wear. Both the oscillations and the variation are getting most significant as soon as the sleeper passing frequency coincides with a frequency of free vertical oscillations of a stationary wheel set on the rail. In early studies of the wheel–rail interaction, the rail inertia and shear

E-mail address: Belotserk1936@rambler.ru.

0022-460X/$ - see front matter
doi:10.1016/j.jsv.2006.03.054

Nomenclature

b_0	bogie base
b_1	distance depending on the bogie frame rotation inertia
c_0, r_0	stiffness and damping of the bogie primary suspension per wheel
$f_0(t)$, $F_0(T)$	dimension/dimensionless contact force
h, H	dimension/dimensionless distance between wheels
k_c	contact spring stiffness
l	sleeper spacing
m_0	unspung mass per wheel
m_1	mass of the bogie frame per wheel
t, T	dimension/dimensionless time
x, X	beam(rail) longitudinal dimension/dimensionless co-ordinate
$y_0(t)$, $Y_0(T)$	wheel dimension/dimensionless vertical deflection
$y(x,t)$, $Y(X,T)$	rail dimension/dimensionless upward deflection
$y(x)$, $Y(X)$	beam dimension/dimensionless transverse deflection
A	cross-section area
EJ	beam(rail) bending stiffness
$R = k'GA$	beam shear stiffness
U	stiffness of uniform elastic foundation

Greek letters

φ	angle of the beam cross-section rotation
σ, S	dimension/dimensionless distribution parameter
$\delta(x)$	Dirac delta-function
v_0	train speed

deformation in the cross-section were disregarded [1,2]. The track static stiffness was calculated and approximated as a sum of a constant and a cosine function. In such a way, the differential equation of the wheel vertical oscillations reduces to the Mathieu equation [3], supplemented with a constant in the right-hand side. There are some differences between such parametric oscillations and forced oscillations due to the rail track roughness. For example, in presence of viscous damping, forced oscillations are always bounded, but, in the same case, solutions to Mathieu equation can be unlimited if the damping is small [4].

Calculations of the single wheel parametric oscillations due to sleeper spacing show significant variation in the normal contact force over the sleeper span at the wheel speed near 120 km/h and the corresponding sleeper passing frequency near 40 Hz [5]. The frequency of such parametric oscillations is low. Therefore, the sleeper and ballast can be presented with a single concentrated mass supported by a spring and a dashpot in parallel. In order to make comparison, the calculations have been made with and without taking into account shear deformation in the rail cross-section. In the second case, the variation in the contact force over the sleeper span turned out to be much less. Thus, the shear deformation strongly influences the parametric oscillations and so the calculations, made in Refs. [1,2] without considering this, remarkably underestimate the wheel parametric oscillations. The Timoshenko beam properties are considered in Section 2.

Interaction among multiple-in-line wheels via the railway track is studied in Sections 3–9. The vertical oscillations of an infinite row of wheels, uniformly moving over the track at the same distance, are calculated by means of a Fourier series technique. If the distance between the wheels is small enough, then their interaction via the track is significant. Otherwise, one can disregard it. In this case, however, the Fourier series technique represents an appropriate approximation conformed to the Fourier integral transformation technique that has been adopted in Ref. [5] to describe the vertical oscillations of a single wheel. As shown in Section 3, such an analytical approach is similar to Ripke's numerical approach to rail–wheel interaction [6]. Any numerical simulation of wheel–rail interaction supposes the railway track length to be finite. Therefore, one has to impose some boundary conditions on the track. Two different boundary conditions were imposed in Ref. [6]. Both of them are also considered in this study.

The tandem wheels interact both via the bogie frame or the vehicle body and via the track. The interaction via the track of four wheels, related to bogies of adjacent vehicles, was investigated in Refs. [7,8]. The distance between the front wheel and the rear wheel of the same bogie is small and the interaction between these wheels both via the rail and via the bogie frame is important. The primary suspension between the wheels and the bogie frame is usually relatively stiffer and the secondary between the frame and the vehicle body is softer.

This makes possible removal of the secondary suspension and replacement of the vehicle body with the static load to simplify the further study. The full investigation can be made in the same way.

2. Timoshenko beam properties

Two consequences follow from Timoshenko beam theory. The first is an additional inertia force due to the shear deformation. The well-known Timoshenko equations of the beam free oscillations take into account this additional inertia force and give a small correction to Euler–Bernoulli theory [9]. These two equations describe the oscillations in terms of the beam transverse deflection and cross-section rotation. The second less known but more important consequence is a discontinuity of the beam centre-line slope at any point where a concentrated transverse force is applied. This force is an idealization usually used to replace a load distributed over a small area. The discontinuity replaces the beam small segment of big curvature. To show this, a single equation that governs the beam transverse deflection will be first derived.

Fig. 1 shows a small beam segment bounded by two cross-sections x and $x+\mathrm{d}x$ and loaded with the distributed moment $m(x)\,\mathrm{d}x$ and transverse force $q(x)\,\mathrm{d}x$. The positive directions of the bending moment M and two angles of rotation φ and $\mathrm{d}y(x)/\mathrm{d}x$, related to the beam cross-section and the centre-line $y(x)$, are also shown. Under the action of the force Q, the rectangular beam segment turns into the parallelogram (see Fig. 1), while the angle between the segment adjacent sides changes its value by $\gamma = Q/R$. The value $R = k'GA$ is the beam shear stiffness, G is the shear modulus, A is the beam cross-section area. The dimensionless coefficient k' accounts for an uneven distribution of the force Q over the beam cross-section. Values M, φ, γ and $\mathrm{d}y(x)/\mathrm{d}x$ are bound with the following equalities:

$$\mathrm{d}y(x)/\mathrm{d}x = \varphi - \gamma = \varphi - Q/R, \qquad M = EJ\,\mathrm{d}\varphi/\mathrm{d}x. \tag{2.1}$$

The value EJ is the beam bending stiffness, E is the modulus of elasticity, J is the moment of inertia of the beam cross-section. Consecutive differentiating and taking into account equalities $q(x)\,\mathrm{d}x - \mathrm{d}Q = 0$ and $m(x)\mathrm{d}x + \mathrm{d}M - Q\,\mathrm{d}x = 0$ of equilibrium of the beam segment give

$$\frac{\mathrm{d}^2y(x)}{\mathrm{d}x^2} = \frac{M}{EJ} - \frac{q(x)}{R}, \quad \frac{\mathrm{d}^3y(x)}{\mathrm{d}x^3} = \frac{1}{EJ}\left(R\left(\varphi - \frac{\mathrm{d}y(x)}{\mathrm{d}x}\right) - m(x)\right) - \frac{\mathrm{d}q(x)}{R\,\mathrm{d}x} \tag{2.2}$$

and yield the following single equation that governs the Timoshenko beam transverse deflection:

$$\frac{\mathrm{d}^4y(x)}{\mathrm{d}x^4} - \frac{1}{EJ}\left(q(x) - \frac{\mathrm{d}m(x)}{\mathrm{d}x}\right) + \frac{\mathrm{d}^2q(x)}{R\,\mathrm{d}x^2} = 0. \tag{2.3}$$

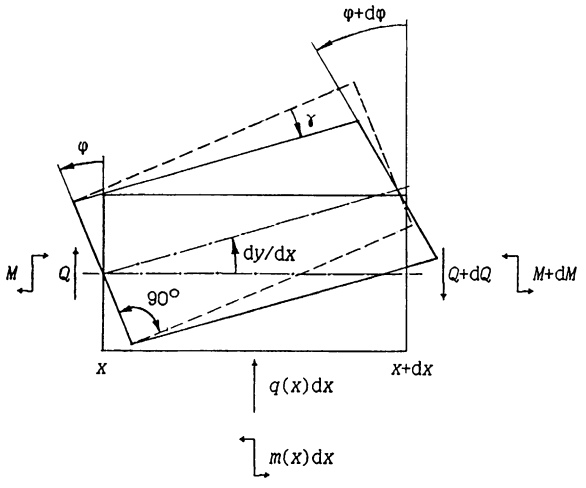

Fig. 1. Bending and shear deformations in a beam.

Further, consider an infinite beam resting on uniform elastic foundation of stiffness u. The distributed foundation reaction is $-uy(x)$. The beam considered bears a downward distributed load $q(x) = -a_0 f(x)$, where a_0 is a positive factor (in N) and the function

$$f(x) = \frac{1}{\sigma\sqrt{2\pi}} \exp\left(-\frac{x^2}{2\sigma^2}\right)$$

yields to the Gaussian normal distribution (see Fig. 2) where σ is the distribution parameter (in m). The value a_0 is the total load applied to the infinite beam, 68% of this total load is applied to the beam segment $-\sigma \leqslant x \leqslant \sigma$. This segment can be compared to the contact patch size; 99.7% of the total load is applied to the greater segment $-3\sigma \leqslant x \leqslant 3\sigma$.

The greatest density of the load corresponds to $x = 0$; its value $q(0) = -a_0/(\sigma\sqrt{2\pi})$ (in N/m) tends to infinity as $\sigma \to 0$ along with those two segments. In this case, the distributed load turns into a concentrated one. The Gaussian normal distribution function $f(x)$ also turns into a Dirac delta-function $\delta(x)$. Substitute $q(x)-uy(x)$ for $q(x)$ in Eq. (2.3). To make calculations easy, the following dimensionless variables and parameters are used only in this section:

$$X = x\sqrt[4]{u/(EJ)}, \quad Y = y\sqrt[4]{u/(EJ)}, \quad S = \sigma\sqrt[4]{u/(EJ)}, \quad A_0 = a_0/\sqrt{EJu}, \quad B = \sqrt{EJu}/R.$$

Now, the differential equation (2.3) takes the following dimensionless form:

$$\frac{\mathrm{d}^4 Y(X)}{\mathrm{d}X^4} - B\frac{\mathrm{d}^2 Y(X)}{\mathrm{d}X^2} + Y(X) = -A_0\left(1 - B\frac{\mathrm{d}^2}{\mathrm{d}X^2}\right)F(X), \quad F(X) = \frac{1}{S\sqrt{2\pi}} \exp\left(-\frac{X^2}{2S^2}\right). \tag{2.4}$$

All solutions to this equation as well as their derivatives of any even order represent even functions. The rest derivatives are odd. Solve Eq. (2.4) by means of Fourier integral transformation technique. To this end, write the direct and inverse transforms in the following form:

$$Y^*(\Omega) = \int_{-\infty}^{+\infty} Y(X)\exp(-\mathrm{i}\Omega X)\,\mathrm{d}X, \quad Y(X) = \frac{1}{2\pi}\int_{-\infty}^{+\infty} Y^*(\Omega)\exp(\mathrm{i}\Omega X)\,\mathrm{d}\Omega.$$

The transform of the Gaussian normal distribution function $F(X)$ equals $\exp(-\Omega^2 S^2/2)$ [4]. Calculate $Y^*(\Omega)$ and substitute it in the inverse transform. Consecutive differentiating yields

$$\frac{\mathrm{d}^j Y(X)}{\mathrm{d}X^j} = \frac{-A_0}{2\pi}\int_{-\infty}^{+\infty} \frac{(\mathrm{i}\Omega)^j(1 + B\Omega^2)\exp(\mathrm{i}\Omega X - \Omega^2 S^2/2)\,\mathrm{d}\Omega}{\Omega^4 + B\Omega^2 + 1}, \quad j = 0, 1, 2, \ldots. \tag{2.5}$$

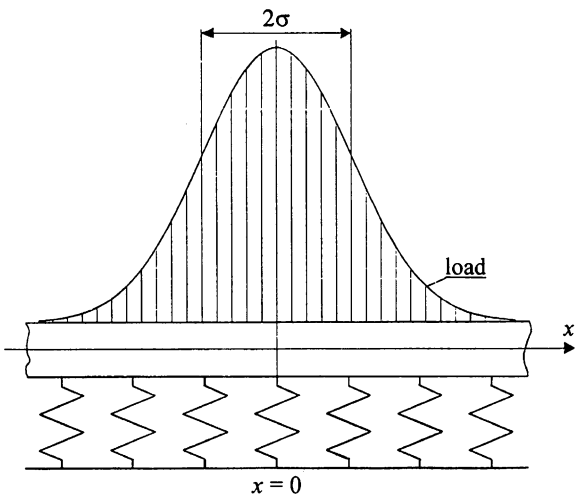

Fig. 2. Beam on uniform elastic foundation.

In the case of distributed load ($S>0$), all the infinite integrals (2.5) exist and represent continuous functions. In the case of concentrated load ($S=0$), the integrals do not exist if $j\geqslant 2$. To avoid this difficulty, one can directly calculate the first integral (2.5) by means of residue technique and the rest by differentiation; $Y(X)$ and its first derivative, both written for $X>0$, are

$$Y(X)=-\frac{A_0}{2}\exp(-\alpha X)\left(\frac{1+B}{\sqrt{2+B}}\cos(\beta X)+\frac{1-B}{\sqrt{2-B}}\sin(\beta X)\right),\quad \alpha=\frac{\sqrt{2+B}}{2},\quad \beta=\frac{\sqrt{2-B}}{2},$$

$$\frac{\mathrm{d}Y(X)}{\mathrm{d}X}=\frac{A_0}{2}\exp(-\alpha X)\left(B\cos(\beta X)+\frac{2-B^2}{\sqrt{4-B^2}}\sin(\beta X)\right).$$

The same can be immediately obtained by means of the Fourier transformation technique starting with the concentrated load instead of the distributed one and the Dirac delta-function $\delta(X)$ instead of the Gaussian normal distribution function $F(X)$. Fig. 3 shows the beam dimensionless transverse deflections $Y(X)$ and their slopes $\mathrm{d}Y(X)/\mathrm{d}X$, related to decreasing values 0.4, 0.2 and 0 of the dimensionless distribution parameter S. The curvature of the beam centre-line at $X=0$ increases along with the load density as $S\to 0$. In the limit case $S=0$, the beam centre-line has the discontinuity of slope at $X=0$. The beam transverse deflection $Y(X)$ and its derivative of the second order are even and so they are continuous. The derivatives of the first order and the third order are odd functions. Their values do not tend to zero as $X\to 0$. Therefore, these derivatives are discontinuous. They, respectively, experience the sudden changes of A_0B and $-A_0(1-B^2)$ as soon as the beam dimensionless longitudinal co-ordinate X changes its negative sign for positive one and passes the point where the concentrated load is applied.

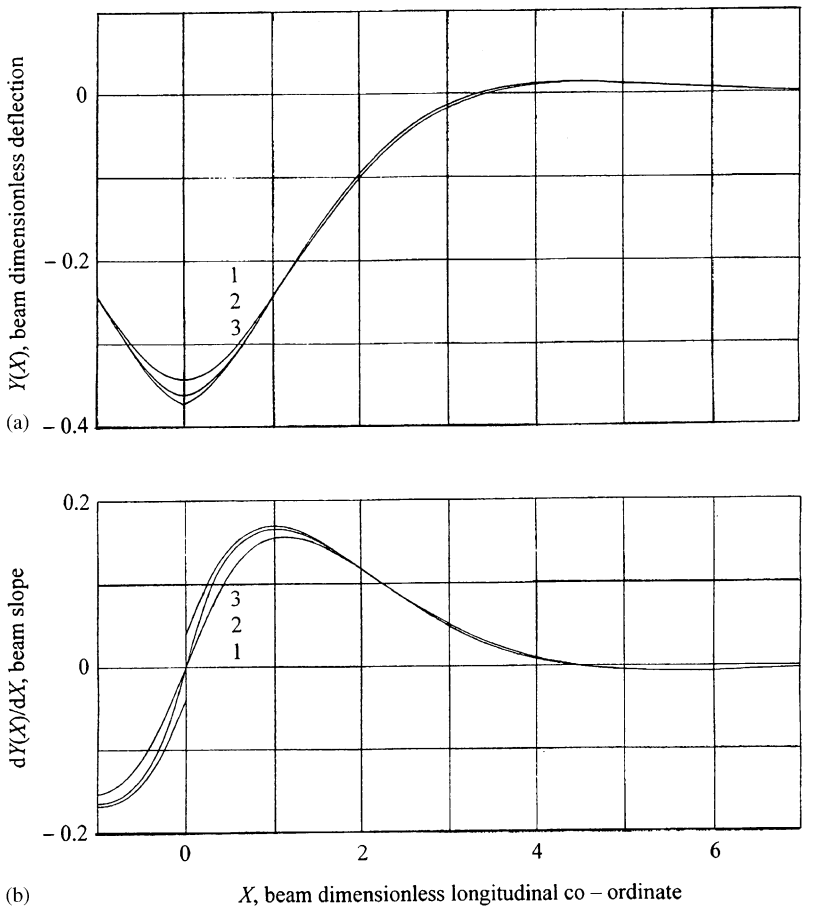

Fig. 3. Beam centre-line: (a) the centre-line deflection; (b) the centre-line slope; 1—$\sigma=0.4$, 2—$\sigma=0.2$, 3—$\sigma=0$.

Return to dimension notation and withdraw the uniform elastic foundation taking $u = 0$. These give two equalities $R[\mathrm{d}y(x)/\mathrm{d}x] = a_0$ and $[\mathrm{d}^3y(x)/\mathrm{d}x^3] = a_0/(EJ)$ where square brackets indicate the difference between the bracketed quantities on either side of the limit x. For example, $[\mathrm{d}y(x)/\mathrm{d}x]$ is $\mathrm{d}y(x+0)/\mathrm{d}x - \mathrm{d}y(x-0)/\mathrm{d}x$. Replace the distributed load $q(x)\mathrm{d}x$ with the concentrated load $-a_0$. Once more taking into account the beam segment equilibrium yields $[Q] = -a_0$.

This gives two equalities

$$R[\mathrm{d}y(x)/\mathrm{d}x] = -[Q], \quad EJ[\mathrm{d}^3y(x)/\mathrm{d}x^3] = [Q] \tag{2.6}$$

that were postulated in Ref. [10]. The first shows that Timoshenko beam centre-line experiences the discontinuity of slope that disappears if R tends to infinity and the beam becomes an Euler–Bernoulli beam. The second shows that both Timoshenko and Euler–Bernoulli beams' centre-lines experience the same sudden change in their third derivatives at a point where a concentrated transverse force is applied. If one calculates the beam transverse deflection by means of Fourier's or similar integral transformation technique and uses the Dirac delta-function, then the equalities (2.6) are automatically taken into account. Otherwise, they should be imposed.

3. Interaction among moving tandem wheels via a rail and Ripke's railway track schemes

Consider a rail as Timoshenko beam of linear density ρ_0. The rail rests on sleepers with spacing l. Each sleeper is modelled as a single concentrated mass ρl, supported by a spring of stiffness ul and a dashpot of viscous damping rl, in parallel. Values ρ, u and r are parameters of the corresponding uniform visco-elastic foundation. Now the rail upward deflection $y(x, t)$ also depends on the time t. Variable x is the longitudinal co-ordinate, let $x = 0$ correspond to a sleeper position. The sleeper at $x = 0$ acts on the rail with reaction $-k(0, t)$, where [5,12]

$$k(0,t) = \rho l\,\partial^2 y(0,t)/\partial t^2 + rl\,\partial y(0,t)/\partial t + uly(0,t). \tag{3.1}$$

Replace values $y(x)$ and $q(x)$ in Eq. (2.3) with $y(x, t)$ and $q(x,t) - \rho_0\,\partial^2 y(x,t)/\partial t^2$, where the first item is an external time-dependent load applied to the rail and the second one represents inertia force due to the rail translation movement. Let value $m(x)$ now represent the distributed moment $-(\rho_0 J/A)\,\partial^2\varphi/\partial t^2$ of inertia force due to the rail cross-section rotation.

Making some usual transformations yields the following partial differential equation:

$$EJ\frac{\partial^4 y(x,t)}{\partial x^4} + \rho_0\frac{\partial^2 y(x,t)}{\partial t^2} - \rho_0\left(\frac{J}{A} + \frac{EJ}{R}\right)\frac{\partial^4 y(x,t)}{\partial x^2\,\partial t^2} + \frac{\rho_0^2 J}{RA}\frac{\partial^4 y(x,t)}{\partial t^4}$$
$$= q(x,t) + \frac{\rho_0 J}{RA}\frac{\partial^2 q(x,t)}{\partial t^2} - \frac{EJ}{R}\frac{\partial^2 q(x,t)}{\partial x^2} \tag{3.2}$$

that governs the rail forced vertical deflection. If the external load is absent, then $q(x, t) = 0$ and the right side of this equation vanishes. In this case, Eq. (3.2) reduces to the well-known single Timoshenko equation of the beam free oscillations [9].

Any numerical simulation of wheel–rail interaction supposes the railway track length h to be finite. Therefore, boundary conditions must be imposed on the track origin and end. Let $x = 0$ corresponds to the origin, the rail track length $h = Hl$, where H is an integer, and $x = h$ corresponds to the rail track end. In Ref. [6], two different conditions $y(h, t) = \pm y(0, t)$ were imposed on the track origin and end. In both cases, one can schematically present the railway track as a ring. In the first case, the ring looks like a *squirrel wheel* (or cage) that is shown in Fig. 4. In the second case, the track rests on *Moebius' surface* shown in Fig. 5. If a steady-state wheel–rail interaction takes place and an analytical simulation is considered, then the ring track can be extended into an infinite track imposing two different periodicity conditions

$$y(x + h, t) = y(x, t), \tag{3.3}$$

$$y(x + h, t) = -y(x, t) \tag{3.4}$$

related to the *squirrel wheel* scheme and *Moebius' surface* scheme. In both cases, one can consider an infinite row of wheels that move with the same constant speed v_0 over the track at the same distance h without

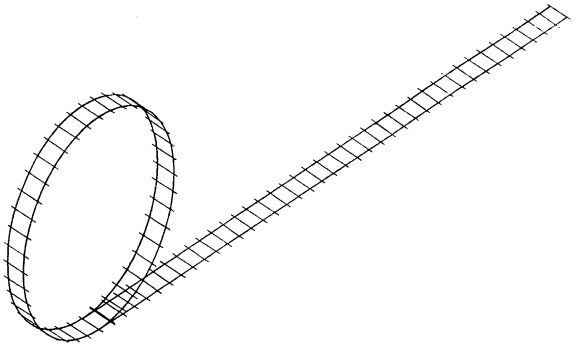

Fig. 4. *Squirrel wheel* scheme.

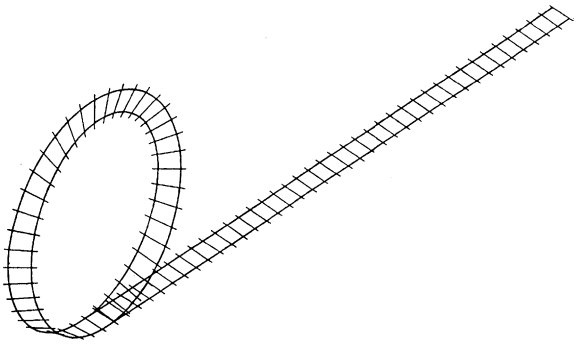

Fig. 5. *Moebius' surface* scheme.

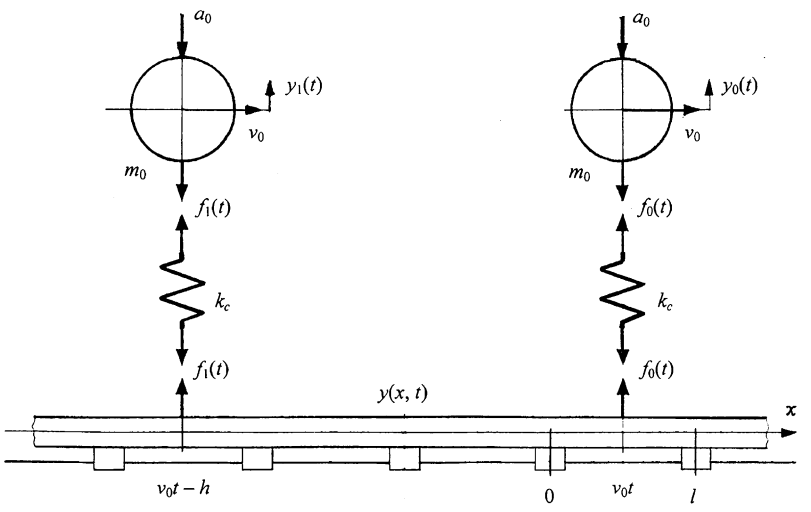

Fig. 6. Row of wheels.

detachment. Every wheel has mass m_0 and links the rail via a linear weightless contact spring having stiffness k_c. The positive direction of the wheel–rail contact force that has period l/v_0, stretches the contact spring and acts contrarily to the wheel and the rail is shown in Fig. 6. Let $t = 0$ correspond to passage of the zero wheel over the point $x = 0$. Present the periodic force between the zero wheel and the rail in the form of

a Fourier series

$$f_0(t) = -a_0 \sum_{n=-\infty}^{+\infty} F_n \exp\left(\frac{\mathrm{i}2\pi n v_0 t}{l}\right), \quad f_0(t + l/v_0) = f_0(t). \tag{3.5}$$

Dimensionless coefficients F_n are unknown. Every item of this series has the same period l/v_0.

In the case of the *squirrel wheel* scheme, every wheel in the row bears the same static downward load (or constant force) of a magnitude a_0 as shown in Fig. 6. In the case of *Moebius' surface* scheme, one can consider the zero wheel to be loaded with the same downward force along with all wheels with an even number and the rest wheels to be loaded with the upward forces of the same magnitude a_0. Further, consider Ripke's railway track schemes separately.

4. Squirrel wheel scheme

Thus, the same equidistant wheels pass over the rail arbitrary point x with the same constant speed. The wheel passing frequency is v_0/h. The first wheel is left behind the zero wheel by time h/v_0. Therefore, the contact forces, related to these two wheels (see Fig. 6), are bound with the following relationship $f_1(t) = f_0(t - h/v_0)$. Repeatedly using this relationship m times, one can conclude that the value $f_0(t - mh/v_0)$ equals the contact force, related to the wheel with number m. Thus, the rail total load due to the infinite row of the same equidistantly moving wheels is

$$q(x, t) = \sum_{m=-\infty}^{+\infty} f_0(t - mh/v_0)\delta(x - v_0 t + mh). \tag{4.1}$$

The Dirac delta-function $\delta(x - v_0 t + mh)$ marks the contact point $x_m = v_0 t - mh$ that corresponds to the wheel with number m. The right-hand side of equality (4.1) does not change if one simultaneously replaces t with $t + h/v_0$ and m with $m + 1$, as well as t with $t + l/v_0$ and x with $x + l$. Thus, the rail total load due to the infinite row of the moving wheels obeys two following periodicity conditions:

$$q(x, t + h/v_0) = q(x, t), \qquad q(x + l, t + l/v_0) = q(x, t).$$

The latter represents a particular case of the more general condition related to a moving harmonic force [5]. Iterating the latter H times yields $q(x + h, t + h/v_0) = q(x, t)$. Then, using the former yields $q(x + h, t) = q(x, t)$. Due to Eq. (3.2), the rail steady-state vertical deflection $y(x, t)$ obeys both periodicity conditions as well as the third expressed in (3.3). Two periodicity conditions $y(x, t + h/v_0) = y(x, t)$ and $y(x + l, t + l/v_0) = y(x, t)$ allow one to restrict the following consideration with the time interval $0 \leqslant t \leqslant h/v_0$ and the rail segment $0 \leqslant x \leqslant l$.

The sleeper reaction considered reduces to the single force $-k(0, t)$ and so the moment M in the rail cross-section is continuous. The force Q in the rail cross-section experiences the sudden change $-k(0, t)$ due to the sleeper reaction at $x = 0$. In accordance with equalities (2.1) and (2.2), the value $-R\partial y(x, t)/\partial x$ does the same, while the following equalities take place:

$$\frac{\partial^2 y(x, t)}{\partial x^2} = \frac{M}{EJ} - \frac{1}{R}\left(q(x, t) - \rho_0 \frac{\partial^2 y(x, t)}{\partial t^2}\right),$$

$$\frac{\partial^3 y(x, t)}{\partial x^3} = \frac{1}{EJ}\left(R\left(\varphi - \frac{\partial y(x, t)}{\partial x}\right) + \frac{\rho_0 J}{A}\frac{\partial^2 \varphi}{\partial t^2}\right) - \frac{1}{R}\left(\frac{\partial q(x, t)}{\partial x} - \rho_0 \frac{\partial^3 y(x, t)}{\partial x \partial t^2}\right).$$

The rail vertical deflection $y(x, t)$, the angle φ of the rail cross-section rotation and their derivatives with respect to t are continuous at $x = 0$. Suppose at this stage that the external load $q(x, t)$ and its derivatives with respect to t are continuous. In accordance with the previous equalities, the value $\partial^2 y(x, t)/\partial x^2$ is continuous, while the following relationship takes place:

$$\frac{EJ}{R}\left[\frac{\partial^3 y(x, t)}{\partial x^3}\right] = -\left[\frac{\partial y(x, t)}{\partial x}\right] + \chi\left[\frac{\partial^3 y(x, t)}{\partial x \partial t^2}\right], \quad \chi = \frac{\rho_0 EJ}{R^2}.$$

The coefficient χ in this relationship is very small and so the last term can be omitted. Thus,

$$EJ[\partial^3 y(x, t)/\partial x^3] = -R[\partial y(x, t)/\partial x] = -k(0, t),$$

The rail deflections $y(0, t)$ and $y(l, t + l/v_0)$ to the left of the adjacent sleepers equal each other. To pose on the segment $0 \leqslant x \leqslant l$ a boundary-value problem for the partial differential equation (3.2), it should be taken into account the values, related to the right of the origin $x = 0$ and to the left of the end $x = l$. Therefore, the following boundary conditions take place:

$$\begin{aligned}
&\partial^j y(l, t + l/v_0)/\partial x^j = \partial^j y(0, t)/\partial x^j, \ \ j = 0, 2,\\
&\partial y(l, t + l/v_0)/\partial x = \partial y(0, t)/\partial x - k(0, t)/R,\\
&\partial^3 y(l, t + l/v_0)/\partial x^3 = \partial^3 y(0, t)/\partial x^3 + k(0, t)/(EJ).
\end{aligned} \tag{4.2}$$

The last two boundary conditions include the above-mentioned sudden change.

Only the zero wheel occurs in the rail segment at the time interval. The infinite sum in the right-hand side of expression (4.1) contains only one non-zero item $f_0(t)\delta(x - v_0 t)$ that corresponds to $m = 0$. Taking into account expression (3.5) yields

$$q(x, t) = -a_0 \sum_{n=-\infty}^{+\infty} F_n q_n(x, t), \quad q_n(x, t) = \exp\left(\frac{\mathrm{i}2\pi n v_0 t}{l}\right)\delta(x - v_0 t). \tag{4.3}$$

Due to linearity of the problem considered, any two loads act on the rail independently from each other and so the rail vertical deflection can be presented in the following form:

$$y(x, t) = -a_0 \sum_{n=-\infty}^{+\infty} F_n y_n(x, t). \tag{4.4}$$

Value $y_n(x, t)$ designates the rail transverse deflection caused by the load $q_n(x, t)$ and obeys the boundary conditions (4.2). Values $y_n(x, t)$ and $q_n(x, t)$ obey Eq. (3.2).

Now proceed to the following new dimensionless variables: the time $T = v_0 t/l$ and the longitudinal co-ordinate $X = x/l$. Note that dimensionless longitudinal co-ordinate, related to the zero wheel $X_0 = x_0/l = v_0 t/l$, coincides with T. Then, take into account that $\delta(l(X - T)) = \delta(X - T)/l$ and $\delta(X - T) = \delta(T - X)$ (see, for example, Ref. [3]). The following dimensionless value $Y_n(X, T) = y_n(x, t)/l$ obeys two periodicity conditions:

$$Y_n(X + 1, T + 1) = Y_n(X, T), \quad Y_n(X, T + H) = Y_n(X, T) \tag{4.5}$$

partial differential equation and boundary conditions

$$\begin{aligned}
&\frac{\partial^4 Y_n(X, T)}{\partial X^4} + \alpha \frac{\partial^2 Y_n(X, T)}{\partial T^2} - (\beta + \gamma) \frac{\partial^4 Y_n(X, T)}{\partial X^2 \partial T^2} + \beta\gamma \frac{\partial^4 Y_n(X, T)}{\partial T^4}\\
&\quad = A_0\left(1 + \psi\left(\beta \frac{\partial^2}{\partial T^2} - \frac{\partial^2}{\partial X^2}\right)\right) \exp(\mathrm{i}2\pi n T)\, \delta(X - T), \quad (0 \leqslant X \leqslant 1),
\end{aligned} \tag{4.6}$$

$$\begin{aligned}
&A_0 = a_0 l^2/(EJ), \quad \alpha = \rho_0 v_0^2 l^2/(EJ), \quad \beta = \rho_0 v_0^2/(EA), \quad \gamma = \rho_0 v_0^2/R, \quad \psi = \gamma/\alpha,\\
&\partial^j Y_n(1, T + 1)/\partial X^j = \partial^j Y_n(0, T)/\partial X^j, \ \ j = 0, 2,\\
&\partial Y_n(1, T + 1)/\partial X = \partial Y_n(0, T)/\partial X - \psi K(0, T),\\
&\partial^3 Y_n(1, T + 1)/\partial X^3 = \partial^3 Y_n(0, T)/\partial X^3 + K(0, T),
\end{aligned} \tag{4.7}$$

$$\begin{aligned}
&K(0, T) = K_2 \partial^2 Y_n(0, T)/\partial T^2 + K_1 \partial Y_n(0, T)/\partial T + K_0 Y_n(0, T),\\
&K_0 = ul^4/(EJ), K_1 = r v_0 l^3/(EJ), K_2 = \rho v_0^2 l^2/(EJ).
\end{aligned}$$

Value $K(0, T)$ is the dimensionless sleeper reaction. In accordance with the second periodicity condition, the dimensionless value $Y_n(X, T)$ can be presented in the form of the following Fourier series:

$$Y_n(X, T) = \sum_{s=-\infty}^{+\infty} C_{s,n}(X) \exp(\mathrm{i}\Phi_s T), \ \ \Phi_s = 2\pi s/H. \tag{4.8}$$

Calculate the unknown Fourier coefficients $C_{s,n}(X)$. To this end, multiply the first periodicity condition (4.5), the partial differential equation (4.6) and the four boundary conditions (4.7) by the factor $\exp(-\mathrm{i}\Phi_s T)\,\mathrm{d}T/H$ and integrate the products with respect to T over the segment $0 \leqslant T \leqslant H$. These integrations are similar to the Fourier integral transformation considered in Section 2. The integration of the partial differential equation automatically takes into account the sudden changes in derivatives of the rail vertical deflection that arise due to the moving vertical concentrated force applied to the rail. The integration gives the following periodicity condition:

$$\exp(\mathrm{i}\Phi_s)C_{s,n}(X+1) = C_{s,n}(X) \tag{4.9}$$

and yields the boundary-value problem for the fourth-order ordinary differential equation

$$\frac{\mathrm{d}^4 C_{s,n}(X)}{\mathrm{d}X^4} + (B+\Gamma)\frac{\mathrm{d}^2 C_{s,n}(X)}{\mathrm{d}X^2} + (B\Gamma - A)C_{s,n}(X) = \frac{A_0}{H}(1+\psi(\Phi_{s,n}^2 - B))\exp(-\mathrm{i}\Phi_{s,n}X) \tag{4.10}$$

with four boundary conditions:

$$\begin{gathered}
\exp(\mathrm{i}\Phi_s)\mathrm{d}^j C_{s,n}(1)/\mathrm{d}X^j = \mathrm{d}^j C_{s,n}(0)/\mathrm{d}X^j,\ \ j = 0, 2,\\
\exp(\mathrm{i}\Phi_s)\mathrm{d}C_{s,n}(1)/\mathrm{d}X = \mathrm{d}C_{s,n}(0)/\mathrm{d}X - \psi K(\Phi_s)C_{s,n}(0),\\
\exp(\mathrm{i}\Phi_s)\mathrm{d}^3 C_{s,n}(1)/\mathrm{d}X^3 = \mathrm{d}^3 C_{s,n}(0)/\mathrm{d}X^3 + K(\Phi_s)C_{s,n}(0),
\end{gathered} \tag{4.11}$$

$$\Phi_{s,n} = \Phi_s - 2\pi n, \quad A = \alpha\Phi_s^2, \quad B = \beta\Phi_s^2, \quad \Gamma = \gamma\Phi_s^2, \quad K(\Phi_s) = -\Phi_s^2 K_2 + \mathrm{i}\Phi_s K_1 + K_0.$$

The polynomial $K(\Phi_s)$ presents the dynamic behaviour of the simplest one-mass support of the rail. Sometimes, high-frequency oscillations (for example, due to rail corrugation) should be considered. In these cases, different parts of the rail support can move diversely. Therefore, the support should be presented with two or more masses (see Ref. [11] for example). The polynomial $K(\Phi_s)$ for such a case can be easily obtained. More complex supports can be included in the study as well. For example, a flexible sleeper can be presented by means of a transcendental function instead of polynomial $K(\Phi_s)$ [12]. To avoid the sudden changes in partial derivatives of the rail vertical deflection, one can replace the Dirac delta-function with the Gaussian normal distribution function (see Section 2 and Appendix A). In theory, the contact patches become infinite and overlap each other. However, the doubled Gaussian normal distribution parameter can be taken as the contact patch size. The replacement results in the appearance of the factor $\exp(-\Phi_{s,n}^2 S^2/2)$ with $S = \sigma/l$ in the right-hand side of Eq. (4.10). This factor is near unity and cannot remarkably influence the results. However, the contact patch size may be important in the case of interaction between corrugated wheels and rails [13,14].

5. Solving the boundary-value problem

Eq. (4.10) has constant coefficients and the exponential function on the right-hand side. It can be solved in usual way [5,12]. The solution determines the Fourier coefficients $C_{s,n}(X)$ only for X belonging to the segment $0 \leqslant X \leqslant 1$. Otherwise, these coefficients can be calculated by means of equality (4.9). If the integer $s = 0$, then $\Phi_s = 0$ too as well as A, B and Γ. In this case, the left-hand side of the differential equation (4.10) retains only the first item. Therefore, two cases $s = 0$ and $s \neq 0$ will be considered separately. A solution to Eq. (4.10) with $s \neq 0$ and the boundary conditions (4.11) is

$$C_{s,n}(X) = A_0\big(\exp(-\mathrm{i}\Phi_{s,n}X) - J(\Phi_s)N(X,\Phi_s)\big)P_{s,n}/H,\ \ 0 \leqslant X \leqslant 1, \tag{5.1}$$

$$\begin{aligned}
N(X,\Phi_s) = {} & \frac{1-\psi\sigma_2^2}{2(\sigma_1^2+\sigma_2^2)}\frac{\sinh(\sigma_1(1-X)) + \exp(-\mathrm{i}\Phi_s)\sinh(\sigma_1 X)}{\sigma_1(\cos\,\Phi_s - \cosh\,\sigma_1)}\\
& - \frac{1+\psi\sigma_1^2}{2(\sigma_1^2+\sigma_2^2)}\frac{\sin(\sigma_2(1-X)) + \exp(-\mathrm{i}\Phi_s)\sin(\sigma_2 X)}{\sigma_2(\cos\,\Phi_s - \cos\,\sigma_2)}\Big),\ \ J(\Phi_s) = \frac{K(\Phi_s)D(\Phi_s)}{K(\Phi_s)+D(\Phi_s)},\\
D(\Phi_s) = 1/N(0,\Phi_s),\ & 2\sigma_{2,1}^2 = ((B-\Gamma)-4A)^{1/2} \pm (B+\Gamma),\ P_{s,n} = (1+\psi(\Phi_{s,n}^2 - B))/L_{s,n}.
\end{aligned}$$

Value $L_{s,n}$ will be defined further. Take into account the following Fourier expansions [5,12]:

$$\exp(\mathrm{i}\Phi_s X)N(X,\Phi_s)=\sum_{m=-\infty}^{+\infty}Q_{s,m}\exp(\mathrm{i}2\pi mX),\ 0\leqslant X\leqslant 1,\ D^{-1}(\Phi_s)=\sum_{m=-\infty}^{+\infty}Q_{s,m},\tag{5.2}$$

$$Q_{s,m}=(1+\psi((\Phi_{s,m}^2-B-\Gamma))/L_{s,m},\ L_{s,m}=\Phi_{s,m}^4-(B+\Gamma)\Phi_{s,m}^2+B\Gamma-A.$$

The last expansion shows that the value $D(\Phi_s)$ is real while the value $K(\Phi_s)$ with any positive damping parameter r is an imaginary one. Thus, if one adopts the integer $s\neq 0$ and any positive r, then the value $K(\Phi_s)+D(\Phi_s)$ does not turn into zero and so the value $J(\Phi_s)$ can be calculated. Substituting the first expansion into the solution (5.1) to the boundary-value problem for the ordinary differential equation (4.10) presents this solution in the next form

$$C_{s,n}(X)=\frac{A_0}{H}\left(\exp(-\mathrm{i}\Phi_{s,n}X)-J(\Phi_s)\sum_{m=-\infty}^{+\infty}Q_{s,m}\exp(-\mathrm{i}\Phi_{s,m}X)\right)P_{s,n}.\tag{5.3}$$

The right-hand side of equality (5.3) complies with the periodicity condition (4.9). Thus, the solution in the last form can be used with any X. Expressions (5.1)–(5.3) become invalid as soon as $s=0$. In this case, $\Phi_{0,n}=-2\pi n$ and the periodicity condition (4.9) reduces to the following equality $C_{0,n}(X+1)=C_{0,n}(X)$ that defines a periodic function whose period equals unity. Now, Eq. (4.10) and boundary conditions (4.11) take the following form:

$$\mathrm{d}^4C_{0,n}(X)/\mathrm{d}X^4=A_0(1+\psi(2\pi n)^2)\exp(\mathrm{i}2\pi nX)/H,\ \ 0\leqslant X\leqslant 1,\tag{5.4}$$

$$\begin{aligned}&\mathrm{d}^jC_{0,n}(1)/\mathrm{d}X^j=\mathrm{d}^jC_{0,n}(0)/\mathrm{d}X^j,\ \ j=0,2,\\&\mathrm{d}C_{0,n}(1)/\mathrm{d}X=\mathrm{d}C_{0,n}(0)/\mathrm{d}X-\psi K_0C_{0,n}(0),\\&\mathrm{d}^3C_{0,n}(1)/\mathrm{d}X^3=\mathrm{d}^3C_{0,n}(0)/\mathrm{d}X^3+K_0C_{0,n}(0).\end{aligned}\tag{5.5}$$

Solving the boundary-value problems (5.4) and (5.5) gives the next two expressions

$$C_{0,n}(X)=A_0P_{0,n}(\exp(\mathrm{i}2\pi nX)-1)/H,\ \ n\neq 0,\tag{5.6}$$

$$C_{0,0}(X)=\frac{A_0}{H}\left(\frac{1}{K_0}+\frac{\psi}{2}X+\frac{1-12\psi}{24}X^2-\frac{1}{12}X^3+\frac{1}{24}X^4\right).$$

The first of them presents the periodic function that complies with the periodicity condition written above and, therefore, can be immediately used with any X. The latter adopts the same value as $X=0$ or 1. Expanding $C_{0,0}(X)$ into a Fourier series gives a periodic function

$$C_{0,0}(X)=\frac{A_0}{H}\left(\frac{1}{K_0}+\frac{\psi}{12}+\frac{1}{720}-\sum_{m\neq 0}P_{0,m}\exp(\mathrm{i}2\pi mX)\right)\tag{5.7}$$

that is valid with any X. Substituting expressions (5.3), (5.6) and (5.7) into equality (4.8) and changing order of summation yield

$$Y_n(X,T)=A_0\sum_{m=-\infty}^{+\infty}\exp(\mathrm{i}2\pi mX)\,W(m,n,T-X),\tag{5.8}$$

$$W(m,n,T-X)=\frac{-1}{H}\sum_{s\neq 0}J(\Phi_s)Q_{s,m}P_{s,n}\exp(\mathrm{i}\Phi_s(T-X)),\ \ m\neq n\neq 0,\tag{5.9}$$

$$W(n,n,T-X)=\frac{1}{H}\sum_{s\neq 0}(1-J(\Phi_s)Q_{s,n})P_{s,n}\exp(\mathrm{i}\Phi_s(T-X)),\ \ n\neq 0,\tag{5.10}$$

$$W(m,0,T-X)=\frac{-1}{H}\left(P_{0,m}+\sum_{s\neq 0}J(\Phi_s)Q_{s,m}P_{s,0}\exp(\mathrm{i}\Phi_s(T-X))\right),\ \ m\neq 0,\tag{5.11}$$

$$W(0,0,T-X)=\frac{1}{H}\left(\frac{1}{K_0}+\frac{\psi}{12}+\frac{1}{720}+\sum_{s\neq 0}(1-J(\Phi_s)Q_{s,0})P_{s,0}\exp(\mathrm{i}\Phi_s(T-X))\right).\tag{5.12}$$

Expressions (5.8)–(5.12) contain some infinite sums that depend on integer-valued variables m, n and s. To make computations in an appropriate way, one should reduce these to the finite sums subject to the following remarks. The discrete variable $\Phi_{s,n} = 2\pi(s/H - n)$ turns into zero as $s = nH$. Therefore, the quantities $L_{s,n}$, $P_{s,n}$ and $Q_{s,n}$, depending on $\Phi_{s,n}$, quickly change their values as soon as the integer-valued variable s passes the integer nH. Thus, the constraints for s should strongly exceed this integer. The integer H determines the distance $h = Hl$ between two adjacent moving wheels whose interaction via the rail track is small enough and so can be disregarded. The integer H must significantly exceed value $|X-T|$. Thus, the computation time consumed to calculate these series increases along with this value.

6. Moebius' surface scheme

Now the wheels loaded with the vertical contrarily directed forces of the same magnitude pass over the rail arbitrary point x with the same constant speed without detachment. Value $(-1)^m f_0(t - mh/v_0)$ equals the contact force, related to the wheel with number m. Thus, the rail total load due to the infinite row of wheels obeys two following periodicity conditions:

$$q(x, t + h/v_0) = -q(x, t), \qquad q(x + l, t + l/v_0) = q(x, t).$$

The rail steady-state vertical deflection $y(x,\ t)$ complies with the similar periodicity conditions that allow one again to pose a boundary-value problem for the partial differential equation (3.2). Proceeding to the dimensionless variables introduced in Section 4 yields again the partial differential equation (4.6) and five boundary conditions. The first $Y_n(X, T + H) = -Y_n(X, T)$ is new, but the rest are the same. Value $Z_n(X, T) = \exp(\mathrm{i}\pi T/H)Y_n(X, T)$ complies with the periodicity condition $Z_n(X, T + H) = Z_n(X, T)$ and so can be presented in the form of the previous Fourier series. Replacing $Z_n(X, T)$ with $Y_n(X, T)$ yields the following equality:

$$Y_n(X, T) = \sum_{s=-\infty}^{+\infty} C^*_{s,n}(X) \exp(\mathrm{i}\Phi^*_s T)$$

that is similar to equality (4.8). New Fourier coefficients $C^*_{s,n}$ obey the same Eq. (4.10) and boundary conditions (4.11) with

$$\Phi^*_s = \Phi_s - \pi/H = \pi(2s - 1)/H, \quad \Phi^*_{s,n} = \Phi^*_s - 2\pi n = \pi(2s - 2n - 1)/H, \quad \Phi^*_{1-s} = -\Phi^*_s.$$

Both Φ^*_s and $\Phi^*_{s,n}$ never equal zero. The coefficients $C^*_{s,n}$ and value $Y_n(X, T)$ obey the same expressions (5.3) and (5.8) that now depend on the variables $\Phi_s = \pi(2s - 1)/H$ and $\Phi_{s,n} = \pi(2s - 2n - 1)/H$ instead of the previous Φ_s and $\Phi_{s,n}$. Only the following two expressions:

$$W(m, n, T - X) = \frac{-1}{H} \sum_{s=-\infty}^{+\infty} J(\Phi_s) Q_{s,m} P_{s,n} \exp(\mathrm{i}\Phi_s(T - X)), \quad m \neq n, \tag{6.1}$$

$$W(n, n, T - X) = \frac{1}{H} \sum_{s=-\infty}^{+\infty} (1 - J(\Phi_s) Q_{s,n}) P_{s,n} \exp(\mathrm{i}\Phi_s(T - X)) \tag{6.2}$$

replace the previous four expressions (5.9)–(5.12).

7. Interaction between the wheel and the rail

Further, consider two Ripke's schemes simultaneously. Divide equality (4.4) by l, insert $Y_n(X, T)$ expressed by equality (5.8). Changing the order of summation yields

$$Y(X, T) = y(x, t)/l = -A_0 \sum_{m=-\infty}^{+\infty} \exp(\mathrm{i}2\pi m X) \sum_{n=-\infty}^{+\infty} F_n W(m, n, T - X). \tag{7.1}$$

Values X and T are arbitrary numbers. Substituting T for X yields the following rail dimensionless vertical deflection at the contact point related to the zero wheel:

$$Y(T,T) = -A_0 \sum_{m=-\infty}^{+\infty} \exp(\mathrm{i}2\pi mT) \sum_{n=-\infty}^{+\infty} F_n W(m,n,0). \tag{7.2}$$

The zero wheel experiences the action of the downward load $-a_0$ and the vertical contact force $f_0(t)$ presented in the form of Fourier series (3.5). The following differential equation:

$$m_0 \frac{\mathrm{d}^2 y_0(t)}{\mathrm{d}t^2} = -a_0 + a_0 \sum_{m=-\infty}^{+\infty} F_m \exp\left(\frac{\mathrm{i}2\pi m v_0 t}{l}\right) \tag{7.3}$$

governs the vertical deflection of the zero wheel and has a finite periodic solution that depends on the unknown Fourier coefficients F_m only if $F_0 = 1$. Proceeding to the dimensionless variables yields the following dimensionless vertical deflection of the zero wheel and contact force

$$Y_0(T) = y_0(t)/l = -A_0 \sum_{m\neq 0} \frac{F_m \exp(\mathrm{i}2\pi mT)}{M_0(2\pi m)^2}, \quad M_0 = m_0 v_0^2 l/(EJ), \tag{7.4}$$

$$F_0(T) = f_0(t)l^2/(EJ) = -A_0 \sum_{m=-\infty}^{+\infty} F_m \exp(\mathrm{i}2\pi mT). \tag{7.5}$$

The contact force $f_0(t)$ extends the contact spring and increases its length by $f_0(t)/k_c$. Therefore, this force, the zero wheel and the rail vertical deflections at the contact point are bound with the equality $y_0(t) = y(v_0 t, t) + f_0(t)/k_c$. The dimensionless values $Y_0(T)$, $Y(T,T)$ and $F_0(T)$ presented in the form of series (7.2), (7.4) and (7.5) comply with the following

$$Y_0(T) = Y(T,T) + F_0(T)/K_c, \quad K_c = k_c l^3/(EJ)$$

that is satisfied provided the coefficient attached to the harmonic function $\exp(\mathrm{i}2\pi mT), m \neq 0$, in the left-hand side and such a coefficient in the right-hand side equal each other.

Thus, taking again $F_0 = 1$, yields an infinite set of linear algebraic equations

$$\left(\frac{1}{K_c} - \frac{1}{M_0(2\pi m)^2}\right) F_m + \sum_{n\neq 0} F_n W(m,n,0) = -W(m,0,0), \quad m \neq 0 \tag{7.6}$$

that include the infinite set of unknown Fourier coefficients F_m, $m \neq 0$.

The complex value F_n and the complex value F_{-n} are conjugate. Therefore, the real value

$$F_n \exp(\mathrm{i}2\pi nT) + F_{-n} \exp(-\mathrm{i}2\pi nT)$$

represents the nth harmonics of the dimensionless contact force between the zero wheel and the rail, its amplitude equals $2|F_n|$. Taking into account only N harmonics reduces the infinite set of Eq. (7.6) to a finite system of equations that contain a finite set of unknown Fourier coefficients. Solving the system yields these Fourier coefficients. The greater the integer N is, the greater the accuracy that can be achieved. It is reasonable to take into account waves in the rail centre-line with wavelengths from l/N to Hl to gain the same accuracy.

Thus, the calculations should be made with integers m, n and s complying with the two constraints $-N \leqslant m$, $n \leqslant N$ and $1-NH \leqslant s \leqslant NH$. In accordance with the remarks in Section 6, the last two constraints should be significantly wider. Finally, let $1-2NH \leqslant s \leqslant 2NH$.

8. Interaction among the wheels via the track and comparing two Ripke's schemes

Start with the *squirrel wheel* scheme. Fig. 7 shows the magnitude of the dimensionless amplitude $2|F_n|$, $n = 1, 2$, versus the wheel speed v_0, calculated with $N = 5$ and the following parameters: $EJ = 3.57 \times 10^6\,\mathrm{N\,m^2}$, $A = 0.006\,\mathrm{m^2}$, $\rho_0 = 48\,\mathrm{kg/m}$, $k' = 0.34$, $l = 0.8\,\mathrm{m}$, $u = 40 \times 10^6\,\mathrm{N/m^2}$, $\rho = 43.6\,\mathrm{kg/m}$, $r = 26 \times 10^3\,\mathrm{N\,s/m^2}$ that correspond to light-rail track and the wheel mass $m_0 = 700\,\mathrm{kg}$. Continuous curves correspond to distance $h = 5l$ between two adjacent wheels while dotted curves do to $h = 10l$. Distinction between these curves is due to

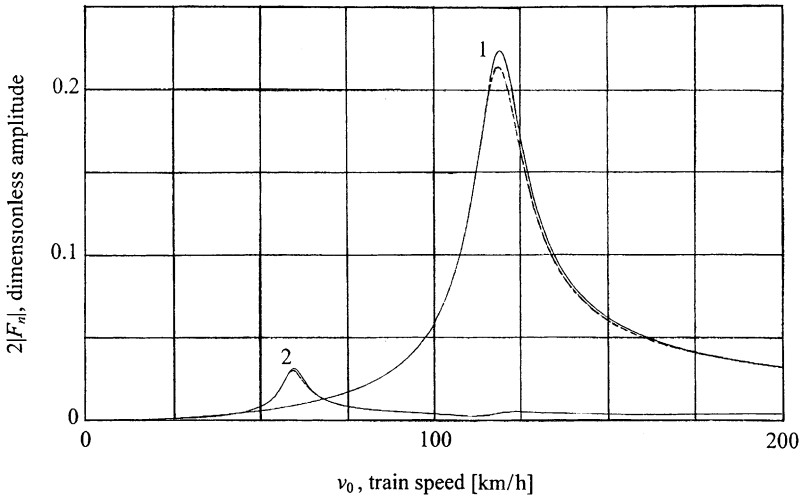

Fig. 7. Contact force dimensionless amplitudes: continuous lines—$h = 5l$, dotted lines—$h = 10l$.

difference in the wheel interaction via the track. Transition to $h = 15l$ causes only a barely visible change in the curve. Thus, the calculations show that the interaction among the wheels via the track can be disregarded as soon as $h \geqslant 10l$. In this case, every wheel in the row can be considered as a single one. Taking $H = h/l = 10$ yields the following constraints: $-99 \leqslant s \leqslant 100$. Thus, only 200 terms should be retained in the series (6.1) and (6.2).

The same results are obtained from the *Moebius' surface* scheme. Since this is simpler it is recommended to describe the interaction between a single moving wheel and the rail. Consider transition from the row of wheels to a single wheel in detail. The discrete variable $\Phi_s = \pi(2s-1)/H$ determines an infinite set of isolated points spaced by distance $2\pi s/H$. The density of these points $H/2\pi$ increases as $H = h/l \to +\infty$. Therefore, the discrete variable Φ_s can be replaced with a continuous variable Φ. Then, the two series (6.1) and (6.2) turn into the two infinite integrals:

$$W(m,n,T-X) = \frac{-1}{2\pi}\int_{-\infty}^{+\infty} J(\Phi)\, Q_m(\Phi)\, P_n(\Phi)\, \exp(\mathrm{i}\Phi(T-X))\,\mathrm{d}\Phi,\ m \neq n,$$

$$W(n,n,T-X) = \frac{1}{2\pi}\int_{-\infty}^{+\infty} (1 - J(\Phi)Q_n(\Phi))\, P_n(\Phi)\, \exp(\mathrm{i}\Phi(T-X))\,\mathrm{d}\Phi,$$

which can be immediately obtained by means of Fourier integral transformation technique [5,12]. In these expressions, the integers m and n play the same role as before. Functions $P_n(\Phi)$ and $Q_n(\Phi)$ replace the similar values $P_{s,n}$ and $Q_{s,n}$. These functions can be calculated in the same way. The following two constraints $-4\pi N \leqslant \Phi \leqslant 4\pi N$ replace the previous ones.

If only oscillations of a single moving wheel are studied, then $T = X$ and the function $\exp(\mathrm{i}\Phi(T-X))$ turns into unity and both the Fourier transformation technique and the Fourier series technique consume the same computation time. In the case of a two-axle bogie, the difference $T-X$ equals the bogie dimensionless base B_0 (see Section 10), a period of that function is $2\pi/B_0$. This period must contain at least eight integration steps d to compute this function. Thus, $d = \pi/(4B_0)$ and the number of the integration steps is $32NB_0$. Let $B_0 = 5$. In this case, the number of the integration steps equals 800 and one needs four times greater computation time. Thus, series (6.1) and (6.2) are the computation time-saving approximation to those integrals.

9. Variation in the rail track static stiffness over a sleeper span

Return to *squirrel wheel* scheme now. Let the parameters ρ_0, ρ and r become zero. Then, the dimensionless parameters A, B and Γ also become zero, while values $K(\Phi_s)$ and $1/D(\Phi_s)$ become K_0 and

$(1-6\psi)/12/(\cos\Phi_s-1)+1/4/(\cos\Phi_s-1)^2$. In this case, the rail deflection is quasi-static. Further, multiply all the items in equalities (7.6) by the dimensionless parameter M_0 and, then, turn the wheel mass m_0 into zero along with M_0. Thus, no inertia force is taken into account in this section. Now equalities (7.6) reduce to the following: $F_m=0$ for all non-zero m while $F_0=1$. Therefore, the equality (5.8) reduces to the next formula

$$Y_0(X_0,X_0)=-A_0\sum_{m=-\infty}^{+\infty}\exp(\mathrm{i}2\pi mX_0)W(m,0,0), \tag{9.1}$$

where the dimensionless time T is replaced with the equal dimensionless co-ordinate X_0 that marks the point, where the constant force applied to the rail. Formula (9.1) leads to the next

$$C(X_0)=-A_0/Y_0(X_0,X_0)=\left(\sum_{m=-\infty}^{+\infty}\exp(\mathrm{i}2\pi mX_0)W(m,0,0)\right)^{-1}. \tag{9.2}$$

Dimensionless value $C(X_0)$ represents the track stiffness per rail at the point X_0.

Fig. 8 shows variation in the dimensionless stiffness $C(X_0)$ over the segment $0\leqslant X\leqslant 1$, related to the sleeper span. Curve 1 presents results of calculations that take into account the shear deformation in the rail cross-section. The greatest value equaled 8.669 is achieved at the points 0 and 1 that correspond to adjacent sleepers. The lowest value, which equals 8.050 and occurs at the point 0.5, relates to the sleeper midspan. The variation in the track stiffness is 0.0741 of the average stiffness. Curve 2 is calculated without taking into account the shear deformation in the rail cross-section. The greatest value equals 8.976 and the lowest is 8.678. The average stiffness slightly increases because the shear deformation is absent, but the relative variation in the stiffness drops to 0.0338 and becomes less than half the previous value. Only the discontinuity of the rail centre-line slope due to the shear deformation in the rail cross-section causes this difference. To reduce the variation in the track stiffness, a similar rail with the greater cross-section area A can be taken. In this case, the rail shear stiffness R increases in proportion to A, while the rail bending stiffness EJ does in proportion to A^2 and so the rail bending deformation quickly reduces. Thus, influence of the shear deformation in the rail cross-section on the variation in the track stiffness over the sleeper span increases.

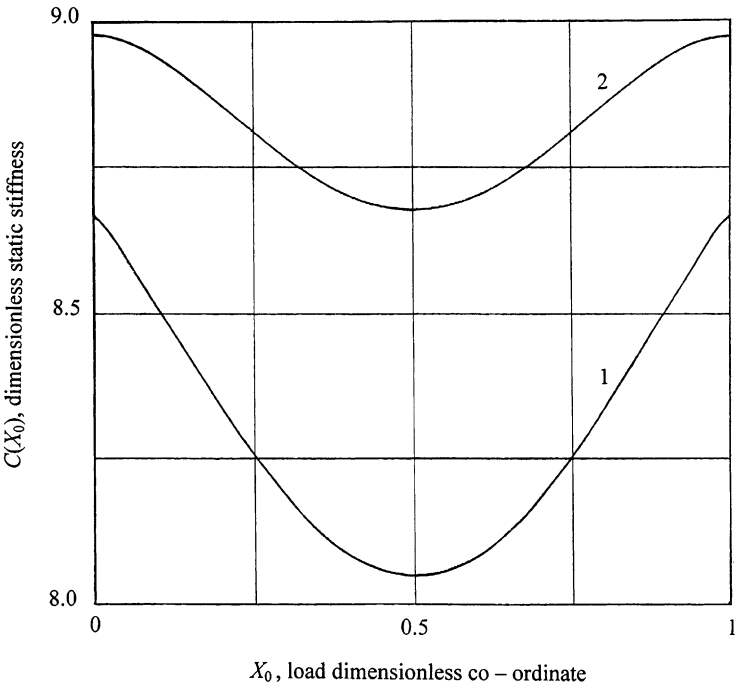

Fig. 8. Variation in the track static stiffness: 1—calculated with taking into account shear deformation in the rail cross-section; and 2—calculated without taking into account shear deformation in the rail cross-section.

10. Bogie vertical deflection and wheel–rail simultaneous oscillations

Fig. 9 shows the simplified bogie model that includes only the primary suspension of stiffness c_0 and damping r_0 per wheel. The frame is modelled with a rigid weightless rod, bearing two masses m_1. Each mass is separated from the other by distance b_1 and presents the frame translation inertia per wheel. The distance b_1 depends on the frame rotational inertia. The wheels are separated by the bogie base b_0. Mass m_0 represents the unsprung mass per wheel; v_0 is the bogie speed and v_0t now denotes the bogie centre position at the time t. Fig. 9 shows positive directions of two periodic contact forces $f^{\pm}(t)$ that relate to the front and rear wheels, pass over the point $x = 0$ at the time $\mp b_0/(2v_0)$ and can be presented in the form of Fourier series

$$f^{\pm}(t) = -a_0 \sum_{n=-\infty}^{+\infty} F_n^{\pm} \exp\left(\frac{\mathrm{i}\pi n(2v_0 t \pm b_0)}{l}\right).$$

As before, a_0 is the static load per wheel, dimensionless coefficients $F_n^{\pm}$ (except $F_0^{\pm} = 1$) are unknown.

Values $y^{\pm}(t)$ present upward periodic deflections from the reference state that relate to the front wheel and the rear wheel. Similarly, values $z^{\pm}(t)$ present the deflections of the rod's front and rear ends. Consider the bogie 'bouncing' and 'galloping' separately. Let

$$f^{\pm}(t) = f_1(t) \pm f_2(t), \quad y^{\pm}(t) = y_1(t) \pm y_2(t), \quad z^{\pm}(t) = z_1(t) \pm z_2(t).$$

The first term in each right-hand side corresponds to the bogie bouncing and the second does to the bogie galloping. In the first case, both wheels oscillate in phase and the bogie frame experiences translation oscillations. Therefore,

$$m_0 \frac{\mathrm{d}^2 y_1(t)}{\mathrm{d}t^2} = -a_0 - f_1(t) + c_0(z_1(t) - y_1(t)) + r_0\left(\frac{\mathrm{d}z_1(t)}{\mathrm{d}t} - \frac{\mathrm{d}y_1(t)}{\mathrm{d}t}\right),$$

$$m_1 \frac{\mathrm{d}^2 z_1(t)}{\mathrm{d}t^2} = -c_0(z_1(t) - y_1(t)) - r_0\left(\frac{\mathrm{d}z_1(t)}{\mathrm{d}t} - \frac{\mathrm{d}y_1(t)}{\mathrm{d}t}\right)$$

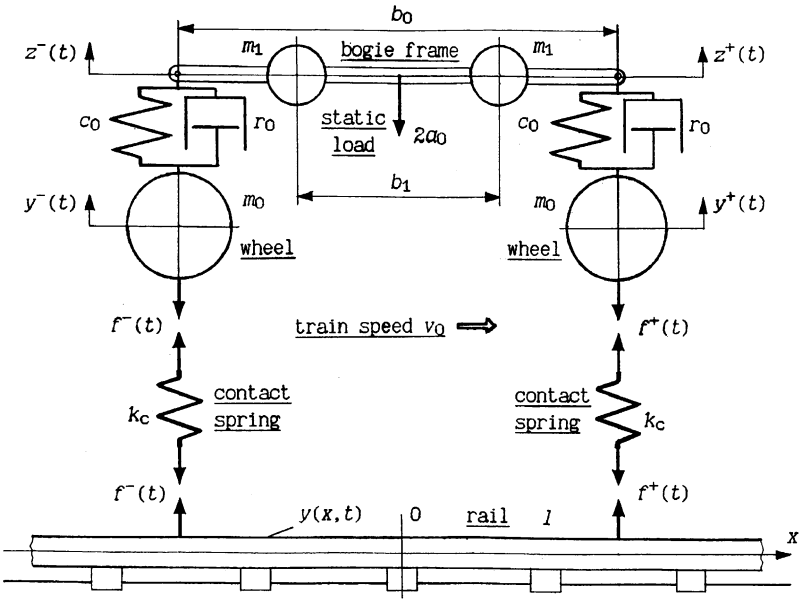

Fig. 9. Simplified bogie model.

which govern the values $y_1(t)$ and $z_1(t)$. Excluding $z_1(t)$ by means of cross differentiation yields a single equation (m is an integer)

$$m_0 m_1 \frac{\mathrm{d}^4 y_1(t)}{\mathrm{d}t^4} + (m_0+m_1) r_0 \frac{\mathrm{d}^3 y_1(t)}{\mathrm{d}t^3} + (m_0+m_1) c_0 \frac{\mathrm{d}^2 y_1(t)}{\mathrm{d}t^2}$$
$$= \frac{a_0}{2} \sum_{m\neq 0} \left(m_1 \left(\frac{2\mathrm{i}\pi m v_0}{l} \right)^2 + r_0 \left(\frac{2\mathrm{i}\pi m v_0}{l} \right) + c_0 \right)$$
$$\times \left(F_m^+ \exp\left(\frac{\mathrm{i}\pi m (2v_0 t + b_0)}{l} \right) + F_m^- \exp\left(\frac{\mathrm{i}\pi m (2v_0 t - b_0)}{l} \right) \right)$$

that contains only the value $y_1(t)$. Substituting $f_2(t)$ and $m_2 = b_1^2 m_1 / b_0^2$ instead of $f_1(t)$ and m_1, one can obtain a similar equation that governs $y_2(t)$. Solving these equations and proceeding to the dimensionless forces $F^{\pm}(T) = f^{\pm}(t) l^2/(EJ)$ and vertical deflections $Y_j(T) = y_j(t)/l$ yield

$$F^{\pm}(T) = -A_0 \sum_{m=-\infty}^{+\infty} F_m^{\pm} \exp(\mathrm{i}\pi m (2T \pm B_0)), \tag{10.1}$$

$$Y_j(T) = -\frac{A_0}{2} \sum_{m\neq 0} W_j(m) \left(F_m^+ \exp(\mathrm{i}\pi m (2T + B_0)) - (-1)^j F_m^- \exp(\mathrm{i}\pi m (2T - B_0)) \right),$$

$$W_j(m) = \frac{M_j (2\pi m)^2 - \mathrm{i} R_0 2\pi m - C_0}{M_0 M_j (2\pi m)^4 - (M_0 + M_j)(2\pi m)^2 (\mathrm{i} R_0 2\pi m + C_0)}, \quad j = 1, 2, \tag{10.2}$$

$$B_0 = b_0/l, \quad C_0 = c_0 l^3/(EJ), \quad R_0 = r_0 v_0 l^2/(EJ), \quad M_j = m_j v_0^2 l/(EJ), \quad j = 0, 1, 2.$$

If $b_1 = b_0$, then $m_2 = m_1$ as well as $M_2 = M_1$ and so $W_1(m) = W_2(m)$. In this case, two masses m_1 that present the bogie frame oscillate independently from each other and so the rigid weightless rod can be removed. Thus, in such a case, the tandem wheels interact only via the track.

Now $y(x, t)$ denotes the rail vertical deflection under the action of the contact forces $f^{\pm}(t)$. Proceeding to the dimensionless values, replacing T by $T \pm B_0/2$ in equality (5.8) and taking into account equality (10.1) yields the following expression:

$$Y(X, T) = -A_0 \sum_{n=-\infty}^{+\infty} \left(F_n^+ Y_n(X, T + B_0/2) + F_n^- Y_n(X, T - B_0/2) \right)$$

providing the rail steady-state dimensionless deflection under the action of the bogie wheels. Taking into account expressions (6.1) and (6.2) and changing order of summation yield

$$Y(X, T) = -A_0 \sum_{m=-\infty}^{+\infty} \exp(\mathrm{i}2\pi m X) \sum_{n=-\infty}^{+\infty} \left(F_n^+ W(m, n, T + B_0/2 - X) + F_n^- W(m, n, T - B_0/2 - X) \right).$$

Two equalities $y^{\pm}(t) = y(v_0 t \pm b_0/2, t) + f^{\pm}(t)/k_c$ bind the contact forces with the vertical deflections of the wheels and the rail at the contact points. Proceed to the dimensionless form

$$Y_1(T) \pm Y_2(T) = Y(T \pm B_0/2, T) + F^{\pm}(T)/K_c, \quad K_c = k_c l^3/(EJ). \tag{10.3}$$

All items in both equalities (10.3) contain values $\exp(\mathrm{i}\pi m(2T \pm B_0))$, multiplied with certain coefficients. These equalities are satisfied if the corresponding coefficients in the left equal the same coefficients in the right. Substituting (10.1) and (10.2) into (10.3) and taking into account $F_0^{\pm} = 1$, yield the

following infinite system of equations:

$$(1/K_c - W_1(m) - W_2(m))F_m^+ - (W_1(m) - W_2(m))F_m^- \exp(-\mathrm{i}2\pi B_0) + \sum_{n\neq 0}(F_n^+ W(m,n,0) + F_n^- W(m,n,-B_0)) = -W(m,0,0) - W(m,0,-B_0)$$

$$-(W_1(m) - W_2(m))F_m^+ \exp(\mathrm{i}2\pi B_0) + (1/K_c - W_1(m) - W_2(m))F_m^- + \sum_{n\neq 0}(F_n^+ W(m,n,B_0) + F_n^- W(m,n,0)) = -W(m,0,0) - W(m,0,B_0)$$

determining an infinite set of Fourier coefficients F_m^+ and F_m^-. Truncating the system and the set yields a finite system, containing N pairs of equations to determine N pairs of the coefficients.

The previous railway track parameters and the following bogie parameters: $m_0 = 700\,\mathrm{kg}$, $m_1 = 500\,\mathrm{kg}$, $c_0 = 3 \times 10^6\,\mathrm{N/m}$, $r_0 = 560\,\mathrm{N\,s/m}$, $b_0 = 1.8\,\mathrm{m}$ and $b_1 = 1.08\,\mathrm{m}$ were used for calculations. Curves 1–3 in Fig. 10 relate to the first, the second and the third dimensionless harmonics of the contact forces. These harmonics have wavelength l/m and the dimensionless amplitudes $2|F_m^{\pm}|$ related to the static load per wheel. The top curves correspond to the front wheel, the bottom curves do to the rear wheel. Curves 1 show that the first amplitude achieves the greatest value that makes up more than 20% the static load per wheel at the main critical speed near 120 km/h. The corresponding sleeper passing frequency is near 40 Hz. A frequency of free vertical oscillations of a stationary wheel set on the rail is near also 40 Hz. The main critical speed corresponds to resonance of a single wheel set on the rail. Thus, the broad peak at the speed near 120 km/h corresponds to the similar peak arising due to interaction between a single wheel and a rail. It is seen an additional sharp resonant peak near 40 km/h and the second near 60 km/h. These peaks relate to the natural frequencies of the bogie frame bouncing and galloping. The wavelengths of the second and the third harmonics of the contact forces, respectively, are 1 s and one-third of the sleeper spacing. Their dimensionless amplitudes achieve the greatest values at 60 and 40 km/h. Due to different wavelengths the corresponding frequency of oscillations is near 40 Hz in both cases. These curves also have the sharp peaks, related to the bogie frame oscillations. The

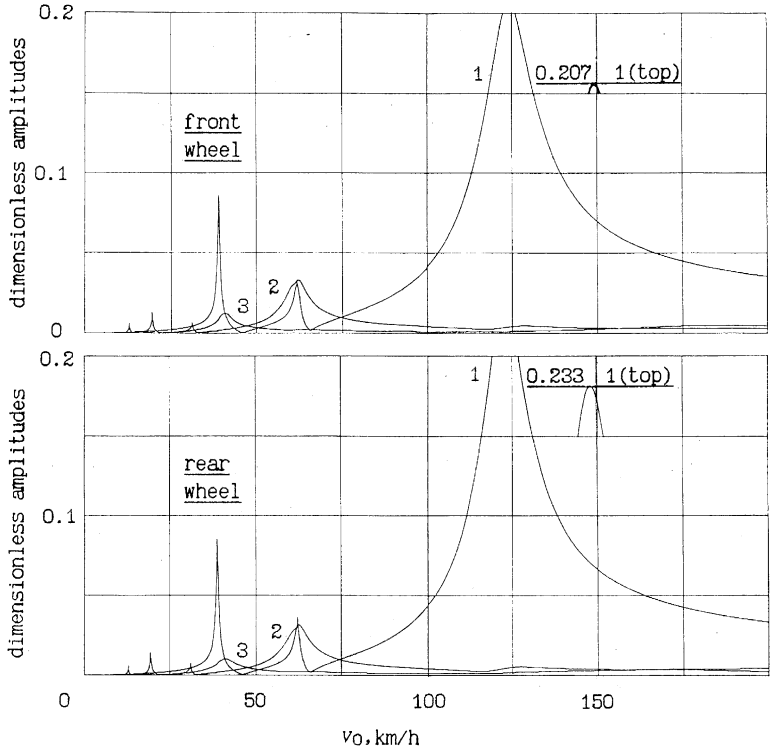

Fig. 10. Wheel–rail contact force amplitudes ($b_1 = 0.6b_0$): 1—$m = 1$, 2—$m = 2$, and 3—$m = 3$.

following presents results of additional calculations undertaken to study dependence on some parameters of the parametric oscillations considered.

Fig. 11 shows similar curves calculated with $b_1 = b_0 = 1.8$ m. In this case, the bogie frame bouncing and galloping have the same natural frequency. Therefore, the above-mentioned two sharp resonant peaks move to the speed 34 km/h and merge. Additional calculations have also shown that the broad peak height strongly depends on the railway track damping while the sharp peak heights strongly depend on the bogie damping. If the bogie damping is great, then these peaks disappear. If the bogie damping slightly exceeds a certain non-zero level, then the peak heights are great. If the damping becomes slightly below this level, then the peaks scatter into many separate points. This takes place due to the parametric nature of the frame oscillations that become unstable in the last case. Another example of instability of a wheel moving with high speed is presented in Ref. [15].

The wheel–rail contact force was calculated by means of expression (10.1). Fig. 12 shows distribution of the downward force over two sleeper spans related to the rear wheel and $b_1 = b_0 = 1.8$ m. Three bold curves mark the sleeper positions. A vertical segment marks the wheel static load. The greatest variation in the contact force relates to the above-mentioned speed 34 km/h. Hollows relate to the greater values of the contact force. Peaks mark the lower values. The hollows are seen on the left of the sleepers and the peaks on the right. The contact force between the rail and the wheel increases as the wheel approaches the sleeper. Then, reduction in the force takes place. In presence of tangential stress, this can cause stick-slip effect and uneven wear both in the rail and in the wheel.

The rail and the wheel are steel and both of them wear out in the same conditions. The rail wear and the wheel wear represent a common process. However, they are usually considered apart [16,17]. The key question is why the rail wear is periodic, but the wheel wear is not at the same time. The track periodicity that provides fixing effect only to the rail and allows wavelengths equal l/m (m is again an integer) seems to be the single answer to this question.

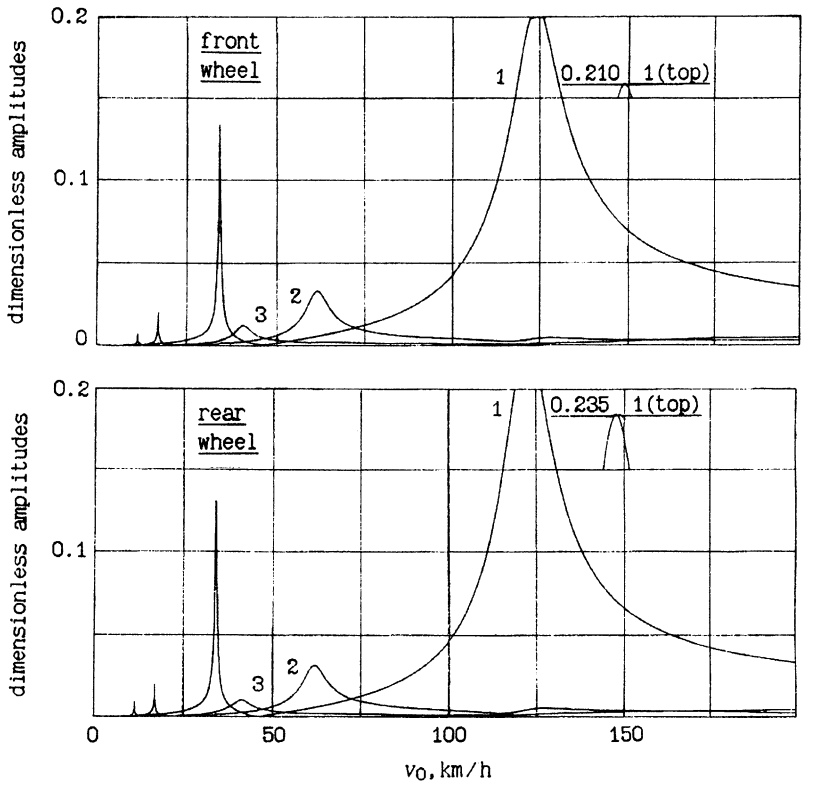

Fig. 11. Wheel–rail contact force amplitudes ($b_1 = b_0$): 1—$m = 1$, 2—$m = 2$, and 3—$m = 3$.

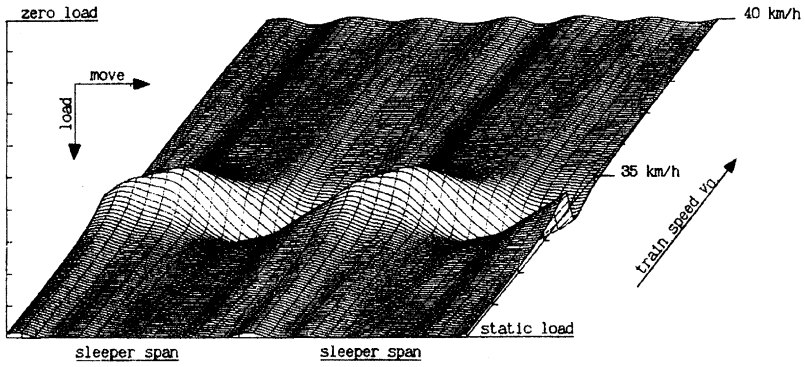

Fig. 12. Wheel–rail contact force variation ($b_1 = b_0$).

11. Conclusions

Timoshenko beam properties were investigated. To this end, a single equation, that governs the beam deflection, was derived. The vertical deflection of an infinite beam that rests on a uniform elastic foundation and bears load conforming to a Gaussian normal distribution was calculated. If the Gaussian distribution parameter tends to zero, then the load becomes concentrated and derivatives of the first and the third order experience a sudden change.

An infinite row of identical wheels that move with the same constant speed over the track at the same distance was considered and interaction among the wheels via the track was estimated. The calculations have shown that the interaction among the wheels via the light-rail track can be disregarded as soon as the distance between two consecutive wheels exceed 10 sleeper spans and so that each wheel in the row can be considered separately.

Interaction between the track and a bogie was studied. The study pointed to the influence of the bogie frame oscillations on variation in the wheel–rail contact force over the sleeper span.

Appendix A

Replace the Dirac delta-function in the right-hand side of equality (3.5) with the Gaussian normal distribution function. Presenting the periodic contact force between the zero wheel and the rail in the form of Fourier series, one can write now

$$f_0(x,t) = -a_0 \sum_{n=-\infty}^{+\infty} F_n \exp\left(\frac{\mathrm{i}2\pi n v_0 t}{l}\right) f(x - v_0 t), \;\; f(x) = \frac{1}{\sigma\sqrt{2\pi}} \exp\left(-\frac{x^2}{2\sigma^2}\right). \tag{A.1}$$

No exponent in the right-hand side of the first equality (A.1) changes its value as the time t increases by h/v_0. As before, the first wheel is left behind the zero wheel by the time h/v_0 and by distance $h = Hl$, H is again an integer. Their contact forces are bound with the relationship

$$f_1(x,t) = f_0(x, t - h/v_0) = -a_0 \sum_{n=-\infty}^{+\infty} F_n \exp\left(\frac{\mathrm{i}2\pi n v_0 t}{l}\right) f(x - v_0 t + h).$$

Repeated usage of this relationship gives the contact force between the rail and an arbitrary wheel in the row. Now, loads from two arbitrary wheels overlap each other. Summarizing these loads and, then, changing the order of summation gives the rail total load due to the infinite row of wheels. Now, the equality (4.1) takes the following form:

$$q(x,t) = -a_0 \sum_{n=-\infty}^{+\infty} F_n \exp\left(\frac{\mathrm{i}2\pi n v_0 t}{l}\right) \sum_{m=-\infty}^{+\infty} f(x - v_0 t + mh)$$

and obeys two previous periodicity conditions. Substitute $q(x, t)$ into the right-hand side of the partial differential equation (3.2). Proceeding to the dimensionless variables from Section 4 yields the following right-hand side of Eq. (4.6)

$$A_0\left(1+\psi\left(\beta\frac{\partial^2}{\partial T^2}-\frac{\partial^2}{\partial X^2}\right)\right)\exp(\mathrm{i}2\pi nT)\sum_{m=-\infty}^{+\infty}F(X-T+mH).$$

The even function $F(X)$ has been defined in Section 2. Now $S=\sigma/l$. To calculate the new right-hand side of Eq. (4.10), multiply the yielded expression by the factor $\exp(-\mathrm{i}\Phi_s T)\,\mathrm{d}T/H$ and integrate the product with respect to T over the segment $0\leqslant T\leqslant H$.

Changing the order of summation and integration gives the following:

$$\frac{A_0}{H}\sum_{m=-\infty}^{+\infty}\int_0^H\exp(-\mathrm{i}\Phi_s T)\left(1+\psi\left(\beta\frac{\partial^2}{\partial T^2}-\frac{\partial^2}{\partial X^2}\right)\right)\exp(\mathrm{i}2\pi nT)F(X-T+mH)\,\mathrm{d}T.$$

Further, one can replace the integration variable T by $T-mH$ in each integral as well as $F(X-T+mH)$ by $F(T-X)$. These replacements do not cause any other change in the integrand. However, the limits of integration change their values by the integer mH. Thus,

$$\begin{aligned}&\frac{A_0}{H}\left(\cdots+\int_{-2H}^{-H}+\int_{-H}^{0}+\int_0^H+\int_H^{2H}+\cdots\right)\exp(-\mathrm{i}\Phi_s T)\left(1+\psi\left(\beta\frac{\partial^2}{\partial T^2}-\frac{\partial^2}{\partial X^2}\right)\right)\exp(\mathrm{i}2\pi nT)F(T-X)\,\mathrm{d}T\\&\quad=\frac{A_0}{H}\int_{-\infty}^{+\infty}\exp(-i\Phi_s T)\left(1+\psi\left(\beta\frac{\partial^2}{\partial T^2}-\frac{\partial^2}{\partial X^2}\right)\right)\exp(\mathrm{i}2\pi nT)F(T-X)\,\mathrm{d}T.\end{aligned}\tag{A.2}$$

All further calculations are valid both for the Gaussian normal distribution function and for the Dirac delta-function. In the last case, the equality

$$\int f(x)\delta^{(j)}(x)\,\mathrm{d}x=(-1)^j f^{(j)}(0)$$

that introduces the derivative for the Dirac delta-function should be taken into account. Make differentiation in the right-hand side of equality (A.2). Introducing the new integration variable $\theta=T-X$ and integrating by parts do that

$$\frac{A_0}{H}\exp(-\mathrm{i}\Phi_s X)\left(1+\psi\Phi_{s,n}^2-\psi\beta((2\pi n)^2+2(2\pi n)\Phi_{s,n}+\Phi_{s,n}^2)\right)\int_{-\infty}^{+\infty}\exp(-\mathrm{i}\Phi_{s,n}\theta)\,F(\theta)\,\mathrm{d}\theta.$$

The last integral has been calculated in Section 2. Making some transformations, the new right-hand side of the ordinary differential equation (4.10) may be stated in the final form

$$\begin{aligned}&\frac{A_0}{H}\exp(-\mathrm{i}\Phi_s X)\left(1+\psi\Phi_{s,n}^2-\psi\beta(\Phi_{s,n}+2\pi n)^2\right)\exp(-\Phi_{s,n}^2S^2/2)\\&\quad=\frac{A_0}{H}\left(1+\psi(\Phi_{s,n}^2-\mathrm{B})\right)\exp(-\mathrm{i}\Phi_s X)\,\exp(-\Phi_{s,n}^2S^2/2).\end{aligned}$$

References

[1] C.E. Inglis, The vertical path of a wheel moving along a railway track, *Journal of Institution of Civil Engineering* 11 (5) (1939) 262–277.

[2] J. Korb, Parametererregung beim Rad-Schiene System, VDI-Fortschritt-Berichte 382, VDI-Verlag, Duesseldorf, 1980, pp. 99–104.

[3] G.A. Korn, T.M. Korn, *Mathematical Handbook for Scientist and Engineers*, McGraw-Hill, New York, 1968.

[4] M. Abramowits, I.A. Stegun, Handbook of Mathematical Functions with Formulas, Graphs and Mathematical Tables, National Bureau of Standards, Applied Mathematical Series 55, 1964.

[5] P.M. Belotserkovskii, The steady vibrations and resistance of railway track to the uniform motion of an unbalanced wheel, *Journal of Applied Mathematics and Mechanics* 67 (5) (2003) 763–773.

[6] B. Ripke, Hochfrequente Gleismodellierung und Simulation der Fahrzeug-Gleis-Dynamik unter Verwendung einer nichtlinearen Kontaktdynamik, VDI Fortschritt-Berichte, Reihe 12, No. 249, VDI-Verlag, Duesseldorf, 1995.

[7] T.X. Wu, D.J. Tompson, Vibration analysis of railway track with multiple wheels on the rail, *Journal of Sound and Vibration* 239 (2001) 69–97.
[8] T.X. Wu, D.J. Tompson, Behaviour of the normal contact force under multiple wheel/rail interaction, *Vehicle System Dynamics* 37 (3) (2002) 157–174.
[9] S.P. Timoshenko, D.H. Young, W. Weaver Jr., *Vibration Problems in Engineering*, Wiley, New York, 1974.
[10] S.P. Timoshenko, *Strength of Materials*, Van Nostrand, New York, 1960.
[11] I. Zobory, V. Zoller, Dynamic response of a periodically supported railway track in case of a moving complex phasor excitation, in: B.G. Teubner (Ed.), Progress in Industrial Mathematics at ECMI 96, Stuttgart, 1997, pp. 85–92.
[12] P.M. Belotserkovskiy, Forced oscillations of infinite periodic structures. Applications to railway track dynamics, *Vehicle System Dynamics Supplement* 28 (1998) 85–103.
[13] T.X. Wu, D.J. Tompson, Theoretical investigation of wheel/rail non-linear interaction due to roughness excitation, *Vehicle System Dynamics* 34 (2000) 261–282.
[14] B. Ripke, K. Knothe, Simulation of high frequency vehicle–track interactions, *Vehicle System Dynamics Supplement* 24 (1995) 72–85.
[15] S.N. Verichev, A.V. Metrikine, Instability of vibrations of a mass that moves uniformly along a beam on a periodically inhomogeneous foundation, *Journal of Sound and Vibration* 260 (2003) 901–925.
[16] Yo. Sato, A. Matsumoto, K. Knothe, Review on rail corrugation studies, *Wear* 253 (2002) 130–139.
[17] J.C.O. Nielsen, R. Lunden, A. Johansson, T. Vernersson, Train–track interaction and measurements of irregular wear on wheel and rail surfaces, *Vehicle System Dynamics* 40 (1–3) (2003) 3–54.